IEEE Access
Multidisciplinary | Rapid Review | Open Access Journal

Received June 5, 2021, accepted June 17, 2021, date of publication June 21, 2021, date of current version June 29, 2021.

Digital Object Identifier 10.1109/ACCESS.2021.3091183

Ambient OFDM Pilot-Aided Backscatter Communications: Concept and Design

TAKANORI HARA, (Graduate Student Member, IEEE), RYUHEI TAKAHASHI, AND KOJI ISHIBASHI, (Senior Member, IEEE)

Advanced Wireless and Communication Research Center (AWCC), The University of Electro-Communications, Tokyo 182-8585, Japan

Corresponding author: Koji Ishibashi (koji@ieee.org)

This work was supported by the Japan Science and Technology Agency (JST), Core Research for Evolutional Science and Technology (CREST) Grant Number JPMJCR20Q1, Japan.

ABSTRACT This paper investigates a backscatter communications system that exploits ambient *pilot* symbols used in existing standards based on *orthogonal frequency-division multiplexing* (OFDM), such as IEEE802.11, in order to realize ultra-low power communications with longer transmission range and higher data rate than conventional ambient backscatter systems. Two modulation schemes, phase-shift keying (PSK) and a new approach named *delay-shift keying* (DSK), are investigated for the proposed system, and the optimal design of DSK is provided based on the theoretical upper bound of the symbol error rate (SER) over double frequency-selective channels. An optimal maximum-likelihood (ML) detector is also developed for the proposed system along with a feasible transmission protocol including channel estimation. Computer simulation results reveal that, at a bandwidth efficiency less than 3 bits per channel use (bpcu), PSK achieves the lowest SER while DSK achieves the lowest SER at efficiencies greater than 2 bpcu. The performance of the proposed detector was comparable to that of the conventional joint ML detectors with a lower degree of complexity, even when a limited number of subcarriers were available as pilot symbols.

INDEX TERMS Ambient backscatter communications (AmBCs), orthogonal frequency-division multiplexing (OFDM), phase-shift keying (PSK), delay-shift keying (DSK), coherent detection, maximum-likelihood (ML) detection, symbol error rate (SER).

I. INTRODUCTION

With the advent of the *internet-of-things* (IoT) era, considerable numbers of battery-driven wireless devices, such as sensors, will be installed, resulting in significant battery replacement costs. To address this, the use of ambient backscatter communications (AmBCs) has been an active focus of research [2]. In [3], a backscatter transmitter (BTx) was proposed and implemented based on an on-off keying (OOK) approach, in which information is transmitted by either reflecting or absorbing *ambient* radio-frequency (RF) signals that are transmitted by existing systems such as IEEE802.11 or TV broadcasting. By implementing OOK with an RF switch, the BTx operated at surprisingly low power levels, e.g., 0.25 μW at 100 bits per second (bps) to 10 kbps. However, it is very difficult for BTx systems to detect AmBCs signals; as a BTx backscatters already-modulated signals from an ambient transmitter (ATx), a backscatter receiver (BRx) must be used to demodulate weakly backscattered signals in the presence of the strong interference produced by the ATx. One strategy for addressing detection problems such as these is to take the average of the received signals over a duration that is longer than the ATx symbol rate to mitigate against the effects of signal fluctuation produced by the ATx modulation [3]. If the symbol rate of the BTx is sufficiently less than that of the ATx, the BRx can extract information by using both a low-path filter (LPW) and an energy detector (ED). Although this simple approach solves the detection problem, it inherently limits the resulting data rate and bandwidth efficiency of AmBC. Another approach is using noncoherent detectors based on maximum-likelihood (ML) detection in AmBCs systems, where BTx adopts coding, e.g., differential coding [4] and Manchester coding [5]. Unlike the aforementioned approach, these detectors suffer from strong interference owing to the direct-link signal.

BackFi, in which an IEEE802.11 access point is assumed as the ATx, was proposed as an approach to increase the bandwidth efficiency in [6]. Under BackFi, the BTx is equipped

The associate editor coordinating the review of this manuscript and approving it for publication was Yiming Huo.

with M different shorted RF terminals and corresponding RF switches. Each RF terminal comprises a transmission line with a unique electrical length. The BTx then transmits information by choosing an adequate RF path to achieve M-ary phase-shift keying (M-PSK). The BackFi BRx is assumed to be co-located with the ATx and to ''perfectly know'' (have complete prior knowledge of) all ambient signals transmitted by the ATx. This enables the BRx to perfectly subtract self-interference from the received signals and demodulate the backscatter signals from the BTx. However, this assumption is not always valid, as some applications can require the separation of the BRx and ATx; in such cases, the BRx will no longer be able to successfully demodulate the signals because it will not be able to detect and cancel ambient signals.

To overcome this limitation, *cooperative AmBC* (CABC) for M-PSK backscattered signals was proposed in [7]. CABC employs a cooperative receiver (CRx) with the ability to detect both backscatter and ambient signals, while the ATx is assumed to use *orthogonal frequency-division multiplexing* (OFDM). The CRx estimates the channel coefficient between itself and the ATx using a pilot signal from the ATx, while the BRx detects information transmitted by the ATx and BTx simultaneously via a joint ML detector or detects the BTx information via successive interference cancellation following the detection of the ATx information. However, the CRx introduces significantly enhanced computational complexity to the BTx signal detection process, which is not preferable in terms of AmBCs power consumption. To mitigate this issue, [8] proposed an ED-based demodulation method. This approach involves the use of a demodulator utilizing multiple EDs; if both the ambient and received signals follow complex, zero-mean Gaussian distributions, which is true if OFDM is employed at the ATx, the ED-based demodulation functions as a multiple hypothesis testing approach based on ML detection. Their numerical results, however, revealed that the ED-based demodulation exhibits a high symbol error rate (SER) error floor in the high signal-to-noise ratio (SNR) region.

There are a few ED-based demodulation schemes that exploit, not the distribution, but the specific structure of an OFDM signal [9]–[11]. According to the scheme proposed in [9], BTx performs the binary backscatter modulation, which takes into account the repeating structure involved in a cyclic prefix (CP) of the OFDM signal, and BRx estimates the backscatter signal via the ED exploiting the structure. In [10], BTx shifts the ambient OFDM signals into the specific in-band null subcarriers to realize M-ary modulation, and BRx extracts information by detecting the energy of backscattered signals taking into account the amount of the spectrum shift. However, BTx in [11] employs M-ary PSK like in [8], and BRx demodulates the backscattered signals by the ED that makes use of whole active-subcarriers of OFDM signals and outperforms the ED proposed in [9]. Although these schemes perform low-complexity detection exploiting the specific structure of the ambient OFDM signals, the detection is *noncoherent* detection, which induces performance loss compared with *coherent* detection. Therefore, an alternative AmBCs approach, which can perform *coherent* detection like in [7], while reducing the detection complexity, is strongly desired to achieve a longer transmission distance between BTx and BRx, which is even more favorable for IoT applications.

Motivated by the aforementioned problems and the relative success of preliminary solutions, we aim to develop a new AmBC system, which can increase the data rate and perform low-complexity coherent detection, to meet the demands of future IoT systems. To this end, we employ a specific OFDM frame structure in current off-the-shelf communications systems, e.g., IEEE 802.11, long-term evolution (LTE), which uses known pilot signals for channel estimation and tracking of channel fluctuations. This structure is already well understood and can therefore be exploited for AmBCs; it has not been utilized in any state-of-the-art system thus far [8]–[11]. Furthermore, we propose a new backscatter modulation scheme called *delay-shift keying* (DSK), which utilizes intentional delays via the designed analog circuits, and demonstrate how to achieve optimal detection using the proposed OFDM pilot-aided AmBCs and theoretically analyze SER performance in a system by applying both PSK and DSK.

The primary contributions of this study are summarized as follows:

- We establish a new AmBC system that, unlike conventional approaches, exploits the use of *pilot* symbols in its ATx-originated OFDM signals. In addition to conventional PSK, the proposed method applies DSK, a tailored backscatter modulation approach. DSK conveys data by adding different propagation delays to produce OFDM symbols with different subcarrier phase rotations within a CP of the ambient OFDM system.
- We propose an optimal ML detector that exploits pilot symbols in ambient OFDM signals to achieve PSK and DSK without requiring demodulation of the ambient signals, resulting in low computational complexity. Because the proposed detector requires multiple channel state information (CSI) corresponding to the direct and reflected paths between the ATx and BRx, we further propose a practical protocol to estimate the associated channel coefficients with the aid of pilot symbols.
- We derive the upper bound of the SER in closed form for the most generalized case, namely for *double frequency-selective channels* in which the channels between both the ATx and BTx and the BTx and BRx are frequency-selective. Based on the results of the SER analysis, we develop an optimal DSK design.
- Based on the results of computer simulations, we demonstrate that PSK achieves the lowest SER at a bandwidth efficiency less than 3 bits per channel use (bpcu), while DSK achieves the lowest SER efficiency at bandwidth efficiencies greater than 2 bpcu. The performance of the proposed detector is comparable to that

of a conventional joint ML detector [7] with reduced complexity, even when limited subcarriers are available as known pilot symbols.

The remainder of this paper is organized as follows. Section II describes the system model used in this study and defines the mathematical representations of PSK and DSK signaling. In Section III, we derive an optimal ML detector for the proposed AmBC and a feasible channel estimation protocol for the detector. We then derive the upper bound of the SER over double frequency-selective channels and provide the DSK design guidelines. In Section V, we demonstrate the performance of the proposed system in terms of SER using computer simulation. Finally, Section VI concludes the paper.

Notations: Lowercase letters, x, boldfaced lowercase letters, $\mathbf{x}$, boldfaced uppercase letters, $\mathbf{X}$, and calligraphic letters $\mathcal{X}$ denote scalars, vectors, matrix variables, and sets, respectively. The Hermitian (conjugate transpose) of a matrix $\mathbf{X}$ is denoted by $\mathbf{X}^{\mathrm{H}}$. We use $\mathbf{I}_N$ to denote the $N \times N$ identity matrix. In addition, $\|\mathbf{x}\|_p$ denotes the ℓ^p norm of a vector $\mathbf{x}$, $|\mathcal{X}|$ denotes the cardinality of a set $\mathcal{X}$, and $\mathcal{CN}(\mu, \sigma^2)$ denotes a circularly symmetric complex Gaussian distribution with mean μ, σ^2.

II. SYSTEM MODEL

Fig. 1 shows a model of an AmBC system comprising single-antenna ATx, BTx, and BRx. It is assumed that the ATx employs OFDM for transmission, and the BRx has perfect knowledge of the pilot symbols transmitted by the ATx. The BTx is equipped with a rectifier for RF energy harvesting to enable self-activation and a backscatter modulator to transmit $\log_2 M$ information bits through either PSK or DSK signaling. Once the BTx has been sufficiently charged, a micro controller switches the antenna connection from the energy harvester to the backscatter modulator, which is described in detail later, and the BTx reflects ambient signals transmitted by the ATx. In this paper, this reflected ambient signal is referred to as a *backscatter signal*.

A. SIGNAL MODEL

We set $(K \times T + 2)$ as the number of OFDM symbols used by the AmBC system, $K \in \mathbb{N}$ as the number OFDM symbols for a backscatter symbol, $T \in \mathbb{N}$ as the number of backscatter symbols in one transmission frame of the BTx, $N \in \mathbb{N}$ as the number of subcarriers, and $N_{\mathrm{c}} \in \mathbb{N}, N_{\mathrm{c}} \leq N$ as the length of each CP, and define $\tilde{s}_k[i] \in \mathcal{A}_a$ as a frequency-domain signal at the i-th subcarrier of the k-th symbol, where $\mathcal{A}_a$ is a modulation alphabet of ambient signals. The time-domain signal transmitted by the ATx at the n-th time sample in the k-th symbol is then given by [12]

$$s_k[n] = \frac{1}{\sqrt{N}} \sum_{i=0}^{N-1} \tilde{s}_k[i] W_N^{-ni}, \quad k = 0, \ldots, KT, KT+1, \tag{1}$$

where $W_N \triangleq e^{-j2\pi/N}$. A transmitted signal with a CP added at the beginning of $s_k[n]$ can then be defined as

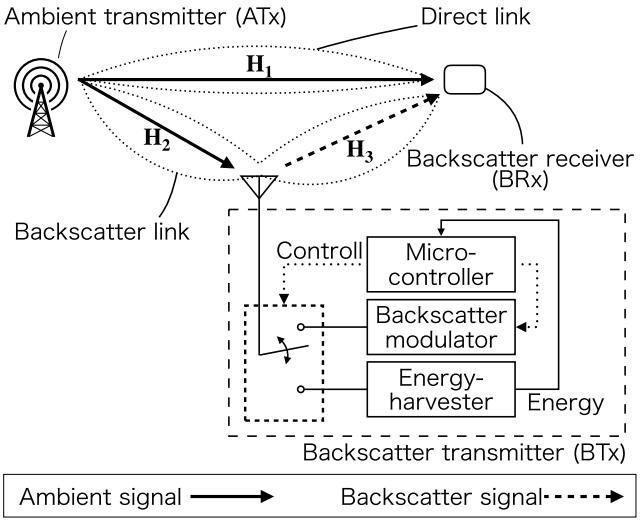

FIGURE 1. System model of ambient backscatter communication.

$s_{k,\mathrm{CP}}[n] \triangleq s[n]_N$ for $n = -N_{\mathrm{c}}, \ldots, N-1$, where $[n]_N$ denotes $[n \mod N]$.

We define $h_1[n] \sim \mathcal{CN}(0, \beta_{1,n})$ as the channel impulse response (CIR) of a channel between the ATx and BRx and $\beta_{1,n}$ as the variance explaining the large-scale fading such in terms of, e.g., path-loss and shadowing. By assuming $(KT+2)$ block-fading (i.e., a constant signal over $(KT+2)$ OFDM symbols), the signal received via the channel from the ATx to the BRx in the k-th symbol duration can be written as [12]

$$y_{\mathrm{d},k}[n] = \sum_{l=0}^{L_1-1} h_1[l] s_{k,\mathrm{CP}}[n-l] = \sum_{l=0}^{L_1-1} h_1[l] s_k[n-l]_N, \tag{2}$$

where L_1 is the number of multi-paths. Here, we refer to $y_{\mathrm{d},k}[n]$ as the signal of a *direct link*.

The BTx also receives an ambient signal expressed as

$$w_{k,\mathrm{in}}[n] = \sum_{l=0}^{L_2-1} h_2[l] s_k[n-l]_N, \tag{3}$$

where $h_2[n] \sim \mathcal{CN}(0, \beta_{2,n})$ is the CIR between the ATx and BTx when there are L_2 multi-paths. Throughout K OFDM symbols, the BTx will reflect the ambient signal $w_{k,\mathrm{in}}[n]$ for backscatter modulation. For a BTx-reflected signal in the time-domain $w_{k,\mathrm{out}}[n]$, the signal received from the BTx at the BRx can be expressed as

$$y_{\mathrm{b},k}[n] = \sum_{l=0}^{L_3-1} h_{3,k}[l] w_{k,\mathrm{out}}[n-l]_N, \tag{4}$$

where $h_3[n] \sim \mathcal{CN}(0, \beta_{3,n})$ is the CIR between the BTx and BRx over L_3 multi-paths. Here, we refer to $y_{\mathrm{b},k}[n]$ as the signal of a *backscatter link*.

The total received signal at the BRx for $n = 0, \ldots, N-1$ and $k = 0, \ldots, KT+1$ can be expressed as

$$y_k[n] = y_{\mathrm{d},k}[n] + y_{\mathrm{b},k}[n] + v_k[n], \tag{5}$$

where $v_k[n] \sim \mathcal{CN}(0, \sigma^2)$ is a zero-mean additive white Gaussian noise (AWGN) with noise power σ^2. The received signal in the frequency domain at the i-th subcarrier is then given by

$$\tilde{y}_k[i] = \frac{1}{\sqrt{N}} \sum_{n=0}^{N-1} y_k[n] W_N^{ni}. \tag{6}$$

To enable the vector representation of the signal model in (6), we define $\tilde{\mathbf{s}}_k \triangleq \left[\tilde{s}_k[0], \cdots, \tilde{s}_k[N-1]\right]^{\mathrm{T}} \in \mathcal{A}_a^{N\times 1}$, $\mathbf{w}_N(n) \triangleq \frac{1}{\sqrt{N}}\left[1, W_N^n, W_N^{2n}, \cdots, W_N^{(N-1)n}\right]^{\mathrm{T}} \in \mathbb{C}^{N\times 1}$, and $\mathbf{v}_k \triangleq [v_k[0], \cdots, v_k[N-1]]^{\mathrm{T}} \in \mathbb{C}^{N\times 1}$. For matrix representation, we further define

$$\mathbf{W} \triangleq \left[\mathbf{w}_N(0) \;\; \mathbf{w}_N(1) \;\; \cdots \;\; \mathbf{w}_N(N-1)\right] \in \mathbb{C}^{N\times N}, \tag{7}$$

$$\mathbf{H}_i \triangleq \begin{bmatrix} h_i[0] & 0 & \cdots & h_i[1] \\ h_i[1] & h_i[0] & \ddots & \vdots \\ \vdots & h_i[1] & \ddots & h_i[L_i-1] \\ h_i[L_i-1] & \vdots & \ddots & 0 \\ 0 & h_i[L_i-1] & \ddots & 0 \\ \vdots & \vdots & \ddots & \vdots \\ 0 & 0 & \cdots & h_i[0] \end{bmatrix} \in \mathbb{C}^{N\times N}, \tag{8}$$

for i = 1, 2, 3. The model can then be rewritten as

$$\tilde{\mathbf{y}}_k = \mathbf{W}\mathbf{H}_1\mathbf{W}^{\mathrm{H}}\tilde{\mathbf{s}}_k + \mathbf{W}\mathbf{H}_3\mathbf{B}_m\mathbf{H}_2\mathbf{W}^{\mathrm{H}}\tilde{\mathbf{s}}_k + \mathbf{W}\mathbf{v}_k, \tag{9}$$

where $\mathbf{B}_m \in \mathcal{A}_\mathbf{B}$ is the $N \times N$ matrix of m-th backscatter modulation and $\mathcal{A}_\mathbf{B}$ of size $|\mathcal{A}_\mathbf{B}| = M$ is an alphabet of the backscatter modulation matrix. Here, we define the SNR as

$$\mathrm{SNR} \triangleq \frac{\mathbb{E}_{\mathbf{H}_2,\mathbf{H}_3,k}\left[\left\|\mathbf{W}\mathbf{H}_3\mathbf{B}_m\mathbf{H}_2\mathbf{W}^{\mathrm{H}}\tilde{\mathbf{s}}_k\right\|_2^2\right]}{\mathbb{E}_k\left[\left\|\tilde{\mathbf{v}}_k\right\|_2^2\right]}, \tag{10}$$

where $\tilde{\mathbf{v}}_k \triangleq \mathbf{W}\mathbf{v}_k$ is the equivalent noise vector in the frequency domain.

B. AMBIENT OFDM PILOT-AIDED BACKSCATTER COMMUNICATIONS

Based on the system model described above, we propose an AmBC system in which, because the BRx knows the structure of the pilots employed in the ATx, the system can exploit subcarriers with known pilots for channel estimation, transmission, and detection. Mathematically speaking, the ARx perfectly knows the pilot symbol $\tilde{s}_k[i]$ in the corresponding i-th subcarrier of the k-th OFDM symbol—knowledge that is not utilized in conventional AmBCs. Without loss of generality and for the sake of brevity of explanation, we assume that the ATx continuously transmits OFDM symbols composed of *only pilot signals* in subsequent sections. This assumption is reasonable because, under the IEEE 802.11 standard, for example, four subcarriers in each OFDM symbol always transmit pilot signals, whereas the first OFDM symbol in the frame transmits only pilots, as illustrated in Fig. 2 [13]. This partial availability of known subcarriers will be discussed in detail in Section V.

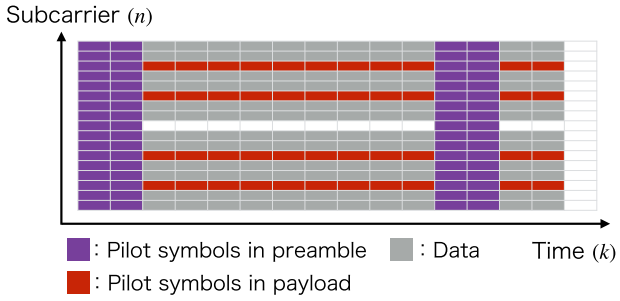

FIGURE 2. Frame structure of IEEE802.11 as an example of an ambient OFDM-based system.

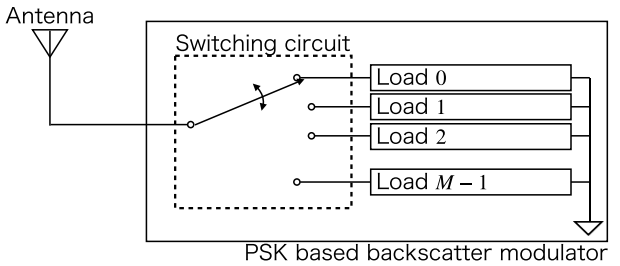

FIGURE 3. PSK-based backscatter modulator comprising M loads with different load impedances.

In the proposed AmBC system, the bandwidth efficiency can be defined as follows

$$R \triangleq \frac{\log_2 M}{K} \text{ [bpcu]}, \tag{11}$$

since K OFDM symbols are utilized for an M-ary backscatter modulated signal. In what follows, we describe two specific backscatter modulations including our proposed modulation named DSK for this AmBC system.

C. BACKSCATTER MODULATOR

The backscatter signal $w_{k,\mathrm{out}}$ and modulation matrix $\mathbf{B}_m$ depend on the BTx modulation scheme. In this section, we investigate the use of PSK and DSK for BTx modulation. In the following analysis, we define the information alphabet as $\mathcal{X} \triangleq \{x_0, \ldots, x_m, \ldots, x_{M-1}\}$ of size $|\mathcal{X}| = M$.

1) PHASE-SHIFT KEYING (PSK)

The proposed modulation scheme is based on the use of impedance-mismatching [8], [14]. As shown in Fig. 3, the PSK-based backscatter modulator comprises a switching circuit and M loads with different impedances. In the BTx, a micro-computer controls a switch connecting the antenna with loads corresponding to each transmission information. If we define Z_A and $Z_{L,m}$ as the impedance of the antenna and the m-th load, respectively, the *reflection coefficient* of

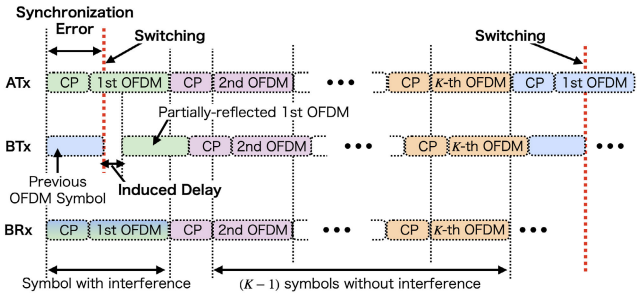

FIGURE 4. Illustration of the effect of imperfect synchronization between ATx and BTx.

the BTx when using the m-th load is given by [8], [14]

$$\Gamma_m \triangleq \frac{Z_{L,m} - Z_A}{Z_{L,m} + Z_A} = |\Gamma_m| e^{j\theta_m}, \tag{12}$$

and the backscatter signal can be expressed as

$$w_{k,\text{out}}[n] = |\Gamma_m| e^{j\theta_m} w_{k,\text{in}}[n]. \tag{13}$$

This backscatter communication process, which is known as *PSK*, can be regarded as a mapping function $l_\theta : \mathcal{X} \to \mathcal{A}_\theta$, where $\mathcal{A}_\theta \triangleq \{\theta_0, \ldots, \theta_m, \ldots, \theta_{M-1}\}$ represents the phase alphabets of BTx.

For simplicity, we assume that the attenuation of each reflection coefficient is $|\Gamma_0| = |\Gamma_1| = \cdots = |\Gamma_{M-1}|$. Then, letting $\alpha_\text{p} \triangleq |\Gamma_0|$, (13) can be rewritten as

$$w_{k,\text{out}}[n] = \alpha_\text{p} e^{j\theta_m} w_{k,\text{in}}[n], \tag{14}$$

and the matrix of PSK modulation can then be defined as

$$\begin{aligned}\mathbf{B}_m &\triangleq \alpha_\text{p} \begin{bmatrix} e^{j\theta_m} & 0 & \cdots & 0 \\ 0 & e^{j\theta_m} & \cdots & 0 \\ \vdots & \vdots & \ddots & \vdots \\ 0 & 0 & \cdots & e^{j\theta_m} \end{bmatrix} \in \mathbb{C}^{N\times N} \\ &= \alpha_\text{p} e^{j\theta_m}. \end{aligned} \tag{15}$$

Note that (15) implies that the transmission of the BTx is synchronized to the ambient OFDM signals. If the ATx and BTx are not synchronized, the switching at the BTx will not occur at the start of the OFDM symbol; instead, it will start arbitrarily at the first symbol of K consecutive OFDM symbols composing one backscatter symbol, as shown in Fig. 4. This synchronization error causes inter-subcarrier interference and inter-symbol interference in the first OFDM symbol, leading to performance degradation. However, this degradation can be easily compensated for by removing the first OFDM symbols at the receiver, resulting in $(K-1)$ OFDM symbols without interference, as depicted in the figure. When K is sufficiently large, the effect of this removal is negligible. This assumption is reasonable because the data rate of the BTx is usually even lower than that of the ATx. In contrast, as the data rate of the backscatter system approaches that of the ATx, this removal is not negligible, thereby requiring more accurate synchronization. In this case, the proposed AmBC system can exploit a practical timing synchronization scheme proposed in [9], which can be performed using a preamble in the ambient OFDM signals. Therefore, in the remainder of this paper, we assume ideal synchronization between the ATx and BTx, which was also assumed in the literature [7], [9], [10].

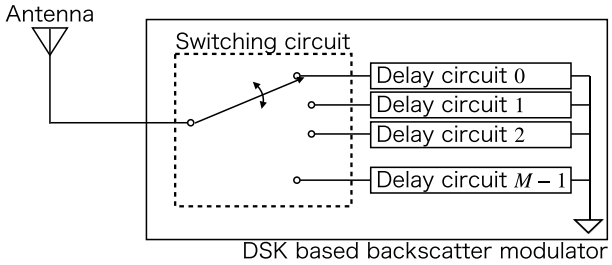

FIGURE 5. DSK-based backscatter modulator comprising M delay circuits with different propagation lengths.

2) DELAY-SHIFT KEYING (DSK)

Fig. 5 shows the DSK-based backscatter modulator, which comprises M delay circuits with different propagation patterns for reflection. Note that these delay patterns can be realized through transmission lines such as surface acoustic wave (SAW) or bulk acoustic wave (BAW) filters, which are widely used in mobile devices in the market as filters at their RF front-ends [15] because of advantages in terms of their small size and light weight. SAW and BAW filters basically operate by first converting the incident electrical signals into acoustic waves through a piezoelectric material, and then converting them back into the electrical waves upon propagation with the speed of sound in the device. As the wavelength in these filters is shorter than that of an electromagnetic guide by a factor of 10^5, such filters can allow for a lower propagation velocity, enabling the delay of hundreds of nanoseconds [16]–[18]. Note that the BAW filters are more suitable than the SAW filters in practice when the center frequency of ambient signals is above 1 GHz [15].

When transmitting information x_m, the BTx reflects $w_{k,\text{in}}[n]$ with a delay of d_m time-samples.[1] We refer to this process as DSK, and it can be regarded as the mapping function $l_d : \mathcal{X} \to \mathcal{A}_\text{d}$, where $\mathcal{A}_\text{d} \triangleq \{d_0, \ldots, d_m, \ldots, d_{M-1}\}$ represent the *delay alphabets* of BTx. For the sake of simplicity, we assume that all the delay circuit attenuation factors are identical; accordingly, the backscatter signal of DSK is given by

$$w_{k,\text{out}}[n] \triangleq \alpha_\text{d} w_{k,\text{in}}[n - d_m], \tag{16}$$

where $\alpha_\text{d} \in [0, 1)$ is an attenuation coefficient of the BTx defined by the insertion loss (attenuation) of SAW or BAW filters. Although this loss depends on their implementation, the typical value has been reported as being less than

[1] To avoid inter-symbol interference, the maximum delay $d_{M-1} + L_2 + L_3 - 2$ at the BRx should not exceed the length of the CP, N_c [13]. The performance of the proposed AmBC system with DSK does not degrade due to the maximum channel delay as long as the condition is satisfied.

2 dB [18]. Thus, the DSK-based modulation matrix $\mathbf{B}_m$ is given by

$$\mathbf{B}_m \triangleq \begin{cases} \alpha_{\mathrm{d}}\mathbf{I}_N & (d_m = 0), \\ \alpha_{\mathrm{d}}\mathbf{T}^{d_m} & (d_m \neq 0), \end{cases} \tag{17}$$

where

$$\mathbf{T} \triangleq \begin{bmatrix} 0 & 0 & \cdots & 0 & 1 \\ 1 & 0 & \cdots & 0 & 0 \\ 0 & 1 & \cdots & 0 & 0 \\ \vdots & \vdots & \ddots & \vdots & \vdots \\ 0 & 0 & \cdots & 1 & 0 \end{bmatrix} \in \{0, 1\}^{N\times N}. \tag{18}$$

Note that, without the time synchronization between the ATx and BTx, the switching of delay circuits may cause inter-subcarrier interference at the first OFDM of the K OFDM symbols corresponding to one DSK symbol. Considering the above discussions, we do not consider this effect and assume ideal synchronization here.

III. FEASIBLE PROTOCOL FOR CHANNEL ESTIMATION AND PILOT-AIDED DETECTION

In this section, we first review the conventional detectors proposed in [7] based on the system model described in the previous section and then describe the optimal ML detector for the proposed AmBC and a feasible channel estimation protocol for the proposed detector. Without loss of generality, we assume $T = 1$ as follows.

A. CONVENTIONAL JOINT ML DETECTOR

For convenience, we let $\mathbf{u} \triangleq [1, 1, \ldots, 1] \in \{1\}^{1\times N}$, $\tilde{\mathbf{H}} \triangleq \mathbf{W}\mathbf{H}_1\mathbf{W}^{\mathrm{H}} + \mathbf{W}\mathbf{H}_3\mathbf{H}_2\mathbf{B}_m\mathbf{W}^{\mathrm{H}} \in \mathbb{C}^{N\times N}$, $\tilde{\mathbf{h}} \triangleq \mathbf{u}\tilde{\mathbf{H}} = [\tilde{h}[0], \ldots, \tilde{h}[N-1] \in \mathbb{C}^{1\times N}$, and $\tilde{h}[i]$ be the i-th element of $\tilde{\mathbf{h}}$. The joint ML (JML) detector is then given by [7]

$$\widehat{\mathbf{B}}_m = \underset{\mathbf{B}_m\in\mathcal{A}_{\mathbf{B}},\tilde{\mathbf{s}}_k\in\mathcal{A}_a^{N\times 1}}{\arg\min} \sum_{k=0}^{K-1} \left\| \tilde{\mathbf{y}}_k - \tilde{\mathbf{H}}\tilde{\mathbf{s}}_k \right\|^2. \tag{19}$$

The number of searches in (19) is $K|\mathcal{A}_{\mathbf{B}}||\mathcal{A}_a|^N$, indicating that a conventional BTx has a high complexity owing to a high number of subcarriers N and a large ambient modulation size $|\mathcal{A}_a|$. To reduce this complexity, we apply the *low-complexity joint maximum-likelihood (L.-C. JML)* detector proposed in [7].

B. CONVENTIONAL LOW-COMPLEXITY JOINT ML DETECTOR

The L.-C. JML detector [7] estimates ambient signals for a given backscatter signal. For a given backscatter signal candidate, (6) can be rewritten as

$$\tilde{y}_k[i] = \tilde{h}[i]\tilde{s}_k[i] + \tilde{v}_k[i], \tag{20}$$

where $\tilde{h}[i]$ is the frequency-domain whole-channel coefficient at the i-th subcarrier, including the backscatter signal, and $\tilde{v}_k[i]$ is the AWGN at the i-th subcarrier at the k-th symbol duration. Using the maximum-ratio-combining method [19], the estimated ambient signal at the i-th subcarrier is obtained as

$$\widehat{\tilde{s}}_k[i] = \underset{\tilde{s}_k[i]\in\mathcal{A}_a}{\arg\min} \left| \frac{\tilde{h}[i]^*}{\left|\tilde{h}[i]\right|^2}\tilde{y}_k[i] - \tilde{s}_k[i] \right|^2. \tag{21}$$

The L.-C. JML detector then estimates the optimal backscatter signal. Setting $\widehat{\tilde{\mathbf{s}}} \triangleq [\widehat{s}_k[0], \ldots, \widehat{s}_k[N-1]]$, the optimal backscatter matrix is given by

$$\widehat{\mathbf{B}}_m = \underset{\mathbf{B}_m\in\mathcal{A}_{\mathbf{B}}}{\arg\min} \sum_{k=0}^{K-1} \left\| \mathbf{y}_k - \tilde{\mathbf{H}}\widehat{\tilde{\mathbf{s}}}_k \right\|^2. \tag{22}$$

Although the number of searches undertaken by the L.-C. JML detector is only $NK|\mathcal{A}_{\mathbf{B}}||\mathcal{A}_a|$, this number grows linearly with the subcarrier and modulation sizes, N and $|\mathcal{A}_a|$, respectively. Accordingly, the proposed pilot-aided detector is designed so that it does not require the estimation of ambient signals.

C. PROPOSED DETECTOR AND CHANNEL ESTIMATION

To accurately detect the backscatter signal, the BRx must eliminate $\mathbf{W}\mathbf{H}_1\mathbf{W}^{\mathrm{H}}\tilde{\mathbf{s}}$ and estimate $\mathbf{H}_2$ and $\mathbf{H}_3$ from (9). To this end, the BTx and BRx use the communication protocol illustrated in Fig. 6, in which each transmission frame is divided into three phases: 1) channel estimation of the direct link, 2) channel estimation of the backscatter link, and 3) data transmission. In phase 1, the BTx connects the antenna with a dummy load to absorb incident signals; as a result, the BRx receives only ambient signals via direct linkage. The signal received by the BRx in this phase is given by

$$\tilde{\mathbf{y}}_{\mathrm{P}_1} = \mathbf{W}\mathbf{H}_1\mathbf{W}^{\mathrm{H}}\tilde{\mathbf{s}} + \mathbf{W}\mathbf{v}_{\mathrm{P}_1}, \tag{23}$$

where $\tilde{\mathbf{s}}$ and $\mathbf{v}_{\mathrm{P}_1}$ are the phase 1 pilot ambient signal and AWGN, respectively. Note that the pilot ambient signal $\tilde{\mathbf{s}}$ is identical in all phases. The BRx estimates $\mathbf{H}_1$ from (23) and leverages $\mathbf{H}_1$ for the subsequent phases. In phase 2, the BTx reflects the ambient signal, which is 0-th backscatter modulated, to the BRx. Thus, the signal received at the BRx in this phase is given by

$$\tilde{\mathbf{y}}_{\mathrm{P}_2} = \mathbf{W}\mathbf{H}_1\mathbf{W}^{\mathrm{H}}\tilde{\mathbf{s}} + \mathbf{W}\mathbf{H}_3\mathbf{B}_0\mathbf{H}_2\mathbf{W}^{\mathrm{H}}\tilde{\mathbf{s}} + \mathbf{W}\mathbf{v}_{\mathrm{P}_2}, \tag{24}$$

where $\mathbf{v}_{\mathrm{P}_2}$ is the AWGN in phase 2. As the modulation matrix $\mathbf{B}_m$ of PSK is given as a scaled identity matrix in (15), for $m = 0, 1, \ldots, M-1$ the product of $\mathbf{B}_m$ and $\mathbf{H}_2$ is obviously commutative. On the other hand, as the modulation matrix $\mathbf{B}_m$ of DSK and $\mathbf{H}_2$ are circulant matrices, $\mathbf{H}_2\mathbf{B}_m = \mathbf{B}_m\mathbf{H}_2$ [20]. Thus, the received signal at the BRx in (24) can be rewritten as

$$\tilde{\mathbf{y}}_{\mathrm{P}_2} = \mathbf{W}\mathbf{H}_1\mathbf{W}^{\mathrm{H}}\tilde{\mathbf{s}} + \mathbf{W}\mathbf{H}_3\mathbf{H}_2\mathbf{B}_0\mathbf{W}^{\mathrm{H}}\tilde{\mathbf{s}} + \mathbf{W}\mathbf{v}_{\mathrm{P}_2}. \tag{25}$$

Although the joint channel matrix $\mathbf{H}_3\mathbf{H}_2$ in (25) cannot be separated [6], by using the estimated $\mathbf{H}_1$ from phase 1, the BRx can estimate $\mathbf{H}_3\mathbf{H}_2$ from (25) instead. Finally, in phase 3 the BTx transmits information to the BRx using PSK or DSK, as shown in (9).

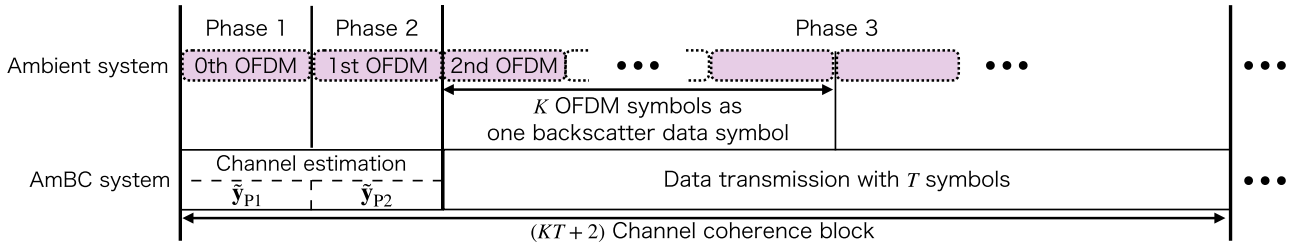

FIGURE 6. Protocol of channel estimation and data transmission under the proposed AmBC system.

Based on the protocol described above, the BRx can obtain channel matrices corresponding to the direct and backscatter links. Based on this, the optimal ML detector for DSK is given by

$$\widehat{\mathbf{B}}_m = \arg\min_{\mathbf{B}_m \in \mathcal{A}_\mathbf{B}} \sum_{k=0}^{K-1} \left\| \tilde{\mathbf{y}}_k - \mathbf{W}\mathbf{H}_1\mathbf{W}^{\mathrm{H}}\tilde{\mathbf{s}} - \mathbf{W}\mathbf{H}_3\mathbf{H}_2\mathbf{B}_m\mathbf{W}^{\mathrm{H}}\tilde{\mathbf{s}} \right\|^2. \tag{26}$$

Because it uses pilot ambient rather than payload signals, it is seen from (26) that the proposed detector uses only $K|\mathcal{A}_\mathbf{B}|$ searches, which is less than what is required under conventional and L.-C. JML detectors [7].

IV. THEORETICAL ANALYSIS AND DESIGN OF DSK

Here, we derive the upper bound of the SER for the proposed AmBC system over double frequency-selective channels under the assumption—based on the application of the protocol described in Section III-C—that the BRx perfectly knows the corresponding CSI. Based on this upper bound, we also provide a design criterion for the DSK.

A. PERFORMANCE BOUNDS OF PROPOSED SYSTEM

We denote transmitted and erroneously decoded signals as $\mathbf{x}_m \triangleq \mathbf{B}_m\tilde{\mathbf{s}}$ and $\tilde{\mathbf{x}}_m \triangleq \mathbf{B}_{\tilde{m}}\tilde{\mathbf{s}}$, respectively, where $\mathbf{B}_m, \mathbf{B}_{\tilde{m}} \in \mathcal{A}_\mathbf{B}$, $m \neq \tilde{m}$. The conditional pairwise error probability (PEP) is given as

$$\Pr\left(\mathbf{x}_m \to \tilde{\mathbf{x}}_m | \mathbf{H}_2, \mathbf{H}_3\right) \triangleq Q\left(\sqrt{2\gamma}\right), \tag{27}$$

where $Q(\cdot)$ is a Gaussian-Q function defined as

$$Q(x) \triangleq \frac{1}{\sqrt{2\pi}} \int_x^\infty \exp\left(-\frac{t^2}{2}\right) dt, \tag{28}$$

and γ is

$$\gamma = \frac{K \cdot \mathrm{SNR}}{4} \left\| \mathbf{H}_3\mathbf{H}_2(\mathbf{x}_m - \tilde{\mathbf{x}}_m) \right\|_2^2, \tag{29}$$

because the matrix $\mathbf{W}$ is a unitary matrix. Applying the Chernoff bound to (27), we obtain

$$\Pr\left(\mathbf{x}_m \to \tilde{\mathbf{x}}_m | \mathbf{H}_2, \mathbf{H}_3\right) \leq \exp\left(-\frac{K \cdot \mathrm{SNR}}{4} d^2(\mathbf{x}_m, \tilde{\mathbf{x}}_m)\right), \tag{30}$$

where $d^2(\mathbf{x}_m, \tilde{\mathbf{x}}_m) \triangleq \left\| \mathbf{H}_3\mathbf{H}_2(\mathbf{x}_m - \tilde{\mathbf{x}}_m) \right\|_2^2$. From this, we obtain the upper bound of the average PEP of the proposed system, i.e., the SER, as

$$P_e \leq \frac{1}{M} \sum_{\mathbf{x}_m} \sum_{\tilde{\mathbf{x}}_m \neq \mathbf{x}_m} \exp\left(-\frac{K \cdot \mathrm{SNR}}{4} d^2(\mathbf{x}_m, \tilde{\mathbf{x}}_m)\right). \tag{31}$$

To simplify the analysis of the SER, we assume a uniform delay power profile and utilize the following approximation [21]:

$$d^2(\mathbf{x}_m, \tilde{\mathbf{x}}_m) \approx \sum_{\ell_2=1}^{L_2} |h_2(\ell_2)|^2 \|\mathbf{H}_3(\mathbf{x}_m - \tilde{\mathbf{x}}_m)\|_2^2. \tag{32}$$

This approximation involves the assumption that $L_2 \geq L_3$, which we can assume without loss of generality here.

We consider the $L_3 \times (N + L_3 - 1)$ matrix $\mathbf{X}_m$, which corresponds to $\mathbf{x}_m$ and is defined by

$$\mathbf{X}_m \triangleq \begin{bmatrix} \mathbf{x}_m^{\mathrm{T}} & 0 & \cdots & 0 \\ 0 & \mathbf{x}_m^{\mathrm{T}} & \ddots & \vdots \\ \vdots & \ddots & \ddots & 0 \\ 0 & \cdots & 0 & \mathbf{x}_m^{\mathrm{T}} \end{bmatrix}. \tag{33}$$

We can then write (32) as

$$d^2(\mathbf{x}_m, \tilde{\mathbf{x}}_m) \approx \sum_{\ell_2=1}^{L_2} |h_2(\ell_2)|^2 \sum_{\ell_3=1}^{L_3} \lambda(\ell_3)|\beta_3(\ell_3)|^2, \tag{34}$$

where $\lambda(\ell_3)$ denote the ℓ_3-th eigenvalues of the matrix $\mathbf{D}(m, \tilde{m}) \triangleq (\mathbf{X}_m - \tilde{\mathbf{X}}_m)(\mathbf{X}_m - \tilde{\mathbf{X}}_m)^{\mathrm{H}} \in \mathbb{C}^{L_3 \times L_3}$ and $\beta(\ell_3)$ are zero-mean complex Gaussian random variables with variance $1/L_3$. Note that, although we should consider a deliberately designed delay of DSK, without loss of generality, we can analyze the performance using the assumption that all pilot symbol elements of the ATx, $\tilde{\mathbf{s}}$, are equal to one as the Euclidean distance is not affected by a unitary transform.

Case 1: $L_2 > L_3$: We first define the random variable $Y = X_1X_2$ with $X_1 = \sum_{\ell_2=1}^{L_2} |h_2(\ell_2)|^2$ and $X_2 = \sum_{\ell_3=1}^{L_3} \lambda(\ell_3)|\beta(\ell_3)|^2$. Substituting (34) into (27) and averaging the resulting expression with respect to Y, we obtain

$$\begin{aligned} \Pr\left(\mathbf{x}_m \to \tilde{\mathbf{x}}_m\right) &\leq \mathbb{E}_Y\left[\exp\left(-\frac{K \cdot \mathrm{SNR}}{4} Y\right)\right] \\ &= \Phi_Y(\omega)\big|_{j\omega = -\frac{K \cdot \mathrm{SNR}}{4}}, \end{aligned} \tag{35}$$

where $\Phi_Y(\omega)$ is the characteristic function of Y. $\Phi_Y(\omega)$ can be evaluated as

$$\Phi_Y(\omega) = \int_0^\infty f_{X_1}(x_1)\Phi_{X_2}(\omega x_1)dx_1, \tag{36}$$

where $f_{X_1}(x_1)$, $x_1 \geq 0$ is the probability density function (PDF) of X_1 and $\Phi_{X_2}(\omega)$ is the characteristic function of X_2, which is expressed as

$$\Phi_{X_2}(\omega)\big|_{j\omega=-\frac{K\cdot\mathrm{SNR}}{4}} = \prod_{\ell_3=1}^{L_3}\left(1+\frac{K\cdot\mathrm{SNR}}{4L_3}\lambda(\ell_3)\right)^{-1} \tag{37}$$

because each $|\beta(\ell_3)|^2$ follows an exponential distribution with the rate parameter L_3. In addition, each $h_2(\ell_2)$ is modeled as a zero-mean complex Gaussian random variable with variance $1/L_2$, and therefore X_1 is a chi-squared random variable with $2L_2$ degrees of freedom.

$$f_{X_1}(x_1) = \frac{L_2^{L_2}}{\Gamma(L_2)}x_1^{L_2-1}e^{-L_2x_1}, \tag{38}$$

where $\Gamma(\cdot)$ is the Gamma function. Therefore, (36) can be written as

$$\Phi_Y(\omega)\big|_{j\omega=-\frac{K\cdot\mathrm{SNR}}{4}} = \frac{L_2^{L_2}}{\Gamma(L_2)}\left(\frac{K\cdot\mathrm{SNR}}{4L_3}\right)^{-L_3} \times \prod_{\ell_3=1}^{L_3}(\lambda(\ell_3))^{-1}\int_0^\infty \frac{x_1^{L_2-1}e^{-L_2x_1}}{\prod_{\ell_3=1}^{L_3}\left(\frac{4L_3}{K\cdot\mathrm{SNR}\cdot\lambda(\ell_3)}+x_1\right)}dx_1. \tag{39}$$

Assuming $K\cdot\mathrm{SNR}/(4L_3) \gg 1$, (39) yields

$$\Phi_Y(\omega)\big|_{j\omega=-\frac{K\cdot\mathrm{SNR}}{4}} = \frac{L_2^{L_2}}{\Gamma(L_2)}\left(\frac{K\cdot\mathrm{SNR}}{4L_3}\right)^{-L_3} \times \prod_{\ell_3=1}^{L_3}(\lambda(\ell_3))^{-1}\int_0^\infty x_1^{L_2-L_3-1}e^{-L_2x_1}dx_1. \tag{40}$$

Using the integral form given by [22, p.346,3.381.4], we obtain

$$\Phi_Y(\omega)\big|_{j\omega=-\frac{K\cdot\mathrm{SNR}}{4}} = L_2^{L_3}\frac{\Gamma(L_2-L_3)}{\Gamma(L_2)}\left(\frac{K\cdot\mathrm{SNR}}{4L_3}\right)^{-L_3}\prod_{\ell_3=1}^{L_3}(\lambda(\ell_3))^{-1}, \tag{41}$$

in which the following relationship is utilized:

$$\int_0^\infty x^{\nu-1}\exp(-\mu x)dx = \frac{1}{\mu^\nu}\Gamma(\nu). \tag{42}$$

By substituting (35) and (41) into (31), we obtain the upper bound of the SER performance of the proposed system for $L_2 > L_3$.

Case 2: $L_2 = L_3$: In this case, the integration in the last term of (40) diverges, and therefore the high-SNR approximation is unusable. Hence, an alternative method to compute $\Phi_Y(\omega)$ is required. Using partial fraction expansion, (39) can be transformed into the following tailored form:

$$\Phi_Y(\omega)\big|_{j\omega=-\frac{K\cdot\mathrm{SNR}}{4}} = \frac{L_2^{L_2}}{\Gamma(L_2)}\left(\frac{K\cdot\mathrm{SNR}}{4L_3}\right)^{-L_3}\prod_{\ell_3=1}^{L_3}(\lambda(\ell_3))^{-1} \times \int_0^\infty x_1^{L_2-1}e^{-L_2x_1}\left[\sum_{n=1}^{N_e}\sum_{i=1}^{m_n}\frac{a_{n,i}}{\left(\frac{4L_3}{K\cdot\mathrm{SNR}\cdot\lambda_n}+x_1\right)^i}\right]dx_1, \tag{43}$$

where N_e, λ_n, and m_n represent the number of unique eigenvalues of $\mathbf{D}(m,\tilde{m})$, the n-th unique eigenvalue, and the geometric multiplicity of λ_n, respectively. After some mathematical manipulation, (43) can be calculated as a summation that includes the exponential-integral function [22, 3.35].

As is apparent from (41) and (43), the diversity order of the proposed system is L_3, which corresponds to a minimum number of path delays. The analysis further implies that the SER performance can be improved linearly with increasing K. As the upper bounds depend on the product of eigenvalues such as the determinant of $\mathbf{D}(m,\tilde{m})$, it is necessary to maximize the determinant to minimize the SER performance. Accordingly, in the next subsection, we discuss the method of designing the DSK delay alphabet in a manner that minimizes the SER.

B. DESIGN OF DELAY ALPHABETS IN DSK

The design of the DSK delay alphabet plays an important role in determining SER performance. Given the assumed structure of $\tilde{\mathbf{s}}$, the head of elements $\mathbf{F}^{\mathrm{H}}\tilde{\mathbf{s}}$ are non-zero while the other elements are zero. Thus, the position of the non-zero element of $\mathbf{x}_m$ is shifted based on the delay d_m.

It is apparent from the structure of $\mathbf{x}_m$ that, if the positions of the non-zero elements in rows $\mathbf{X}_m - \mathbf{X}_{\tilde{m}}$ do not overlap, the off-diagonal elements in $\mathbf{D}(m,\tilde{m})$ vanish and the eigenvalues of $\mathbf{D}(m,\tilde{m})$ become the largest eigenvalues. Hence, all the differences between d_m and $d_{\tilde{m}}$, *i.e.*, $|d_m - d_{\tilde{m}}|$, should at least be more than $L_3 - 1$.

Although the theoretical analysis in the previous subsection ignored the coupling of $\mathbf{H}_2$ and $\mathbf{H}_3$, it revealed that the SER performance can be maximized if all differences between d_m and $d_{\tilde{m}}$ are larger than the number of path delays. Since the maximum path delay is L_2+L_3-2, the criterion for the optimal design of the delay alphabet $\mathcal{A}_\mathrm{d}$ is consequently given by

$$|d_m - d_{\tilde{m}}| > L_2 + L_3 - 2. \tag{44}$$

The validity of this criterion will be confirmed in the next section.

V. NUMERICAL RESULTS

In this section, we evaluate the SER performances of the proposed AmBC system based on the results computer simulations. In the following analysis, we assume perfect channel estimation, and therefore that the channel matrices of the direct and backscatter links are ideally available. Unless

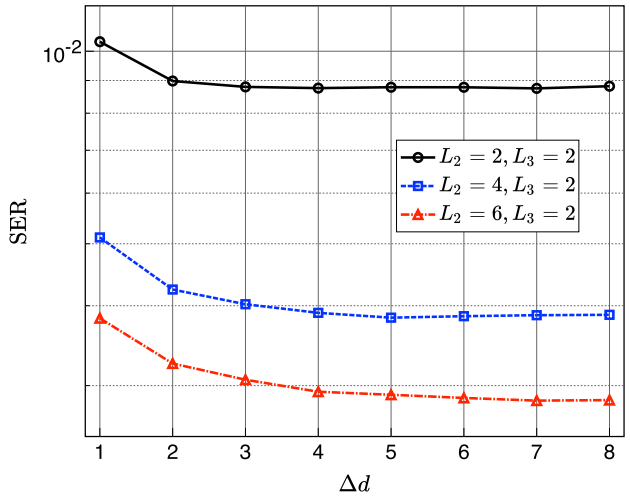

FIGURE 7. SER performance of 4-DSK as a function of Δd.

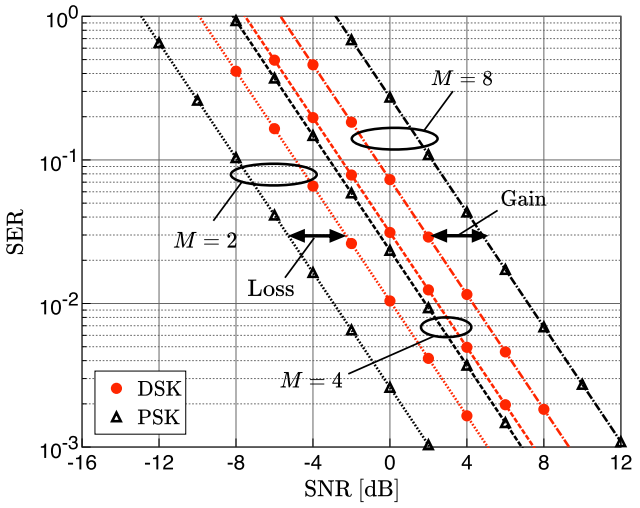

FIGURE 8. Upper bounds of SER performance by proposed AmBC system with $(L_2, L_3) = (4, 2)$.

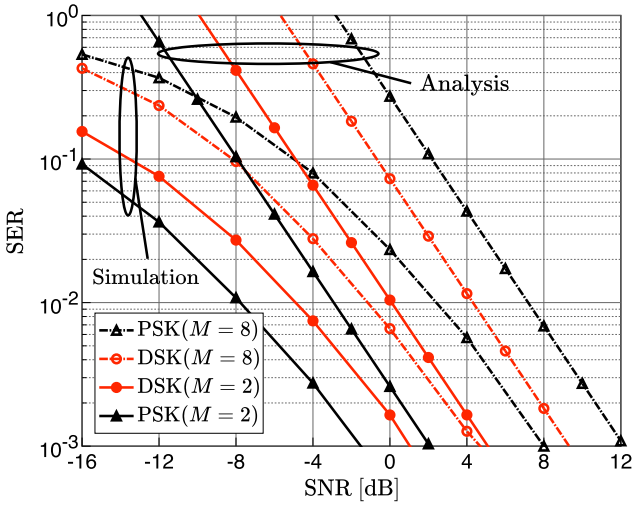

FIGURE 9. SER performance of proposed AmBC system and upper bounds derived in Section IV for $M = 2$ and 8.

otherwise specified, the simulation settings were $N = 64$, $N_c = 16$, $K = 1$, $L_1 = L_2$, and $\alpha_p = \alpha_d = 1$.[2] Furthermore, all channels followed a uniform power delay profile.

A. DSK VS. PSK

We first confirmed the validity of the delay alphabet design criterion. Fig. 7 shows the SER performance of a 4-DSK scheme in terms of the minimum difference defined as $\Delta d \triangleq \min |d_m - d_{\tilde{m}}|$, where $SNR = 0$ dB and N_c are both assumed to be smaller than $d_{M-1} + L_2 + L_3 - 2$. As shown in the figure, the SER for each set of L_2 and L_3 gradually decreased as Δd increased, reaching nearly constant values at $\Delta d > L_2 + L_3 - 2$. These numerical results confirm the validity of the design criterion described in Section IV-B.

Fig. 8 shows the upper bound derived in Section IV for cases in which $L_2 = 4$, $L_3 = 2$, and N_c exceed $d_{M-1} + L_2 + L_3 - 2$ for all M. This result indicates that, although the proposed DSK is inferior to PSK at $M = 2$ and 4, it is robust against increases in M as its performance loss is less than that of PSK. DSK yields the Euclidean distance at the sequence level by modulating all subcarriers; by contrast, PSK arranges only one complex plane. This difference between the two backscatter modulation approaches accounts for the relationship shown in Fig. 8.

We then compared the empirical and theoretical SER performance of the AmBC system using computer simulations. Fig. 9 shows the empirical SER performance of the proposed AmBC system for $M = 2$ and 8 along with the upper bounds derived in Section IV. It is apparent that the theoretical analysis in Section IV accurately derived the upper bound of SER performance of the proposed method. The empirical results showing the relationship between DSK and PSK are given in Fig. 8, from which it is seen that the theoretical analysis presented in this paper is accurate for the case $L_2 > L_3$.

We investigated the SER performance of the proposed AmBC system in the special case for which $L_2 = L_3$. Fig. 10 shows the SER performance of the proposed method with 4-ary modulation at $L_2 = L_3 = 2$. Along with the associated plots, the analytical SERs derived in Section IV are shown in the figure. It is seen from the figure that the analytical performance derived in Section IV provides an accurate upper bound. It is also apparent that the bound in the low-SNR regime is tighter than that in the case $L_2 > L_3$ because the high-SNR approximation is not applied.

We finally discuss the choice of M and K to achieve a given bandwidth efficiency. Fig. 11 shows the empirical and theoretical SER performance of the proposed AmBC system with $M = 2$ and $K = 1$ and with $M = 4$ and $K = 2$ for

[2]Under an AmBC configuration, the BTx is sufficiently close to the BRx, and therefore the distance between the ATx and BRx is slightly longer than that between the ATx and BTx. As a result, the number of paths L_1 and L_2 will in all likelihood be identical.

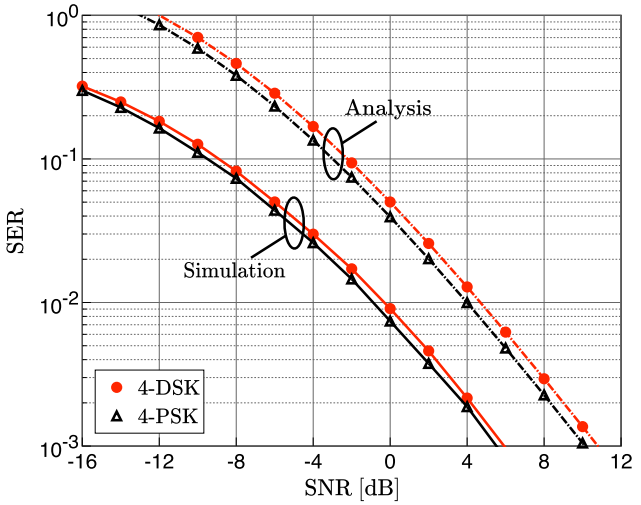

FIGURE 10. SER performance of proposed AmBC system and upper bounds derived in Section IV for $(L_2, L_3, M) = (2, 2, 4)$.

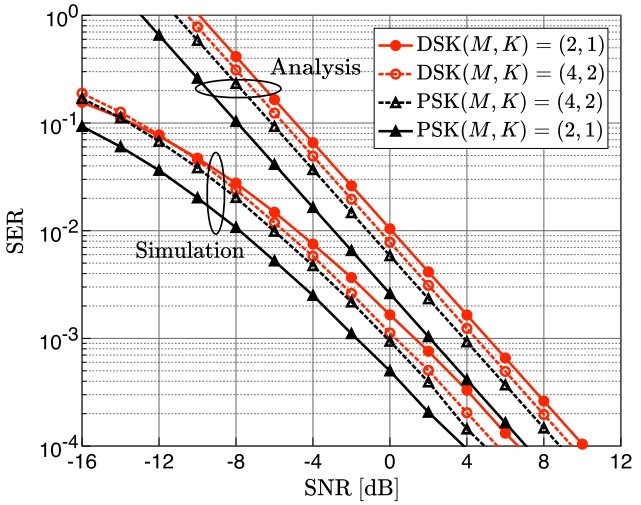

FIGURE 11. SER performance of proposed AmBC system with different combinations of M and K for 1 bpcu.

1 bpcu where the delay alphabet is set to satisfy $\Delta = 4$ for 4-DSK. From the figure, it can be concluded that a smaller M leads to a lower SER performance for both PSK and DSK. This explains that the loss of the minimum Euclidean distance obtained by doubling M is greater than 3 dB, which is obtained by doubling K. Furthermore, an increase in the M is accompanied by an increase in the size of the transmitter, which is not preferable for major applications investigated in this study. We therefore conclude that a minimum value of M must be chosen to achieve a given bandwidth efficiency. Note that K can alleviate the requirement of synchronization between ambient and backscatter systems. Additionally, the value of K should be increased if the number of loads or delay circuits is fixed, and if the application requires a better receiver sensitivity.

The results presented in this subsection demonstrate that our theoretical analysis approach was effective at appropriately designing the delay alphabet and predicting the behavior of the proposed AmBC system for double frequency-selective channels.

B. PROPOSED ML VS. CONVENTIONAL JOINT ML DETECTOR

In this subsection, we compare the SER performance of the proposed AmBC system with that of the conventional AmBC system proposed in [7]. We focus on the case for which $M = 4$ and set the DSK delay alphabet as $\mathcal{A}_\mathrm{d} = \{0, 4, 8, 12\}$. There are assumed to be four pilot subcarriers for the payload and the associated indices are set as 11, 25, 39, and 53 based on IEEE802.11a [13].

The SER performance for the case in which $L_2 = L_3 = 1$, i.e., the case of double flat-fading channels, is shown in Fig. 12, in which the results obtained by the proposed AmBC system exploiting preamble and payload pilot symbols are labeled "Proposed, preamble" and "Proposed payload", respectively. The results obtained by the conventional system employing quadrature PSK (QPSK) and 16-ary quadrature amplitude modulation (16QAM) as ambient modulation are denoted by "L.-C. JML, QPSK" and "L.-C. JML, 16QAM," respectively. For simplicity, these notations are used throughout this subsection. As shown in the figure, in the case in which it exploits preamble pilot symbols, the proposed system significantly outperforms the conventional system and the computational complexity of its optimized ML detector is lower than that of the detector proposed in [7]. Similarly, in the case in which it exploits payload pilot symbols, the proposed system performs comparably to the conventional system in the low-SNR regime. This result suggests that the proposed system can perform in a manner comparable to conventional approaches even when a limited number of subcarriers is available as known pilot symbols.

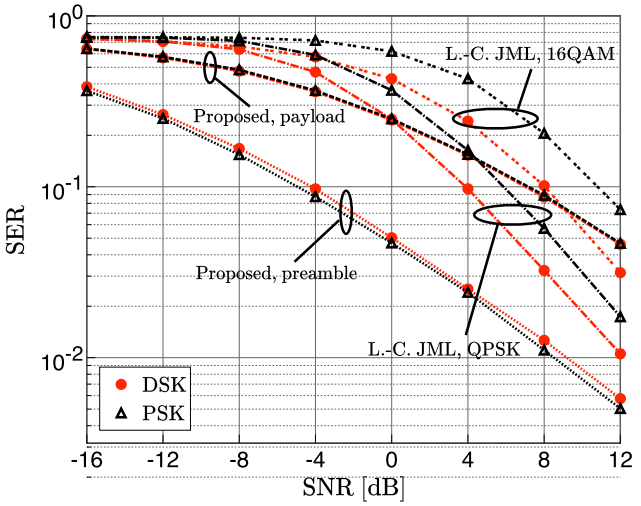

FIGURE 12. SER performances of proposed and conventional AmBC systems with $(M, L_2, L_3) = (4, 1, 1)$.

We then investigated the SER performance of the two approaches over double frequency-selective channels. Fig. 13 shows the SER performance for $(M, L_2, L_3) = (4, 4, 2)$. Note

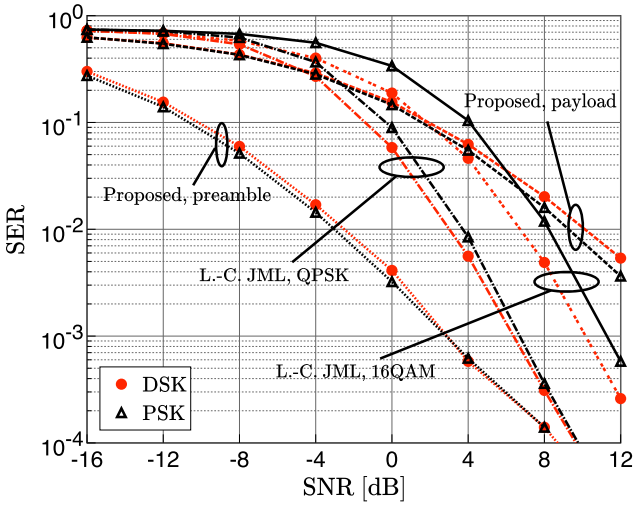

FIGURE 13. SER performance of proposed and conventional AmBC systems with $(M, L_2, L_3) = (4, 4, 2)$.

that the Δd of $\mathcal{A}_{\rm d}$, a factor considered in this subsection, does not satisfy $\Delta > L_2 + L_3 - 2$. However, as is seen from Fig. 7, the performance gap owing to this difference is negligible and the value of Δd can be set to avoid inter-carrier interference, i.e., $d_{M-1} + L_2 + L_3 - 2 \leq N_c$. This result indicates that, when using preamble pilot symbols, the proposed AmBC system can achieve a lower SER than the conventional approach over the entire SNR range. Although the performance gap in the high-SNR regime is smaller than that shown in Fig. 12, the proposed method consistently outperforms the conventional method. However, in exploiting payload pilot symbols, the proposed scheme underperforms the conventional method, as is also demonstrated in the results shown in Fig. 12. Nevertheless, at sufficiently large SER values, the proposed method can utilize payload pilot symbols to a attain a SER below 10^{-2} if the SNR is sufficiently large. This suggests that the proposed AmBC system is capable of achieving superior SER performance even if a few pilot subcarriers, i.e., payload pilot symbols, are used to convey the BTx information.

VI. CONCLUSION

In this paper, we proposed a new AmBC system utilizing a well-understood, OFDM-based ambient system common structure. To implement the proposed AmBC, a feasible transmission protocol for channel estimation and two modulation schemes, PSK and DSK, were investigated and an optimal ML detector with a reduced degree of complexity relative to conventional joint ML detectors was proposed. To design the proposed DSK scheme, the upper bound of its SER performance was derived in a closed form. Numerical results confirmed our theoretical analysis and demonstrated that PSK modulation achieves the lowest SER values at bandwidth efficiencies of less than 3 bpcu while DSK modulation achieves the lowest SER values at bandwidth efficiencies greater than 2 bpcu. As a more practical evaluation condition, we investigated the performance of the proposed method when a limited number of subcarriers is available as pilot symbols and demonstrated that the proposed detector could perform comparably to a conventional method with an ML detector that is less complex than a conventional joint ML detector. The proposed approach can achieve higher bandwidth efficiency with reduced detection complexity and is suitable for use in existing systems that utilize OFDM; therefore, it can be considered a viable option for use in the ultra-low power communications systems of the IoT era.

ACKNOWLEDGMENT

This article was presented in part at the 2019 IEEE Global Conference on Signal and Information Processing (GlobalSIP), Ottawa, Canada [1].

REFERENCES

[1] R. Takahashi and K. Ishibashi, "Ambient OFDM pilot-aided delay-shift keying and its efficient detection for ultra low-power communications," in *Proc. IEEE Global Conf. Signal Inf. Process. (GlobalSIP)*, Nov. 2019, pp. 1–5.

[2] N. Van Huynh, D. T. Hoang, X. Lu, D. Niyato, P. Wang, and D. I. Kim, "Ambient backscatter communications: A contemporary survey," *IEEE Commun. Surveys Tuts.*, vol. 20, no. 4, pp. 2889–2922, 4th Quart., 2018.

[3] V. Liu, A. Parks, V. Talla, S. Gollakota, D. Wetherall, and J. R. Smith, "Ambient backscatter: Wireless communication out of thin air," *ACM SIGCOMM Comput. Commun. Rev.*, vol. 43, no. 4, pp. 39–50, Sep. 2013.

[4] G. Wang, F. Gao, R. Fan, and C. Tellambura, "Ambient backscatter communication systems: Detection and performance analysis," *IEEE Trans. Commun.*, vol. 64, no. 11, pp. 4836–4846, Nov. 2016.

[5] Q. Tao, C. Zhong, H. Lin, and Z. Zhang, "Symbol detection of ambient backscatter systems with Manchester coding," *IEEE Trans. Wireless Commun.*, vol. 17, no. 6, pp. 4028–4038, Jun. 2018.

[6] D. Bharadia, K. R. Joshi, M. Kotaru, and S. Katti, "BackFi: High throughput WiFi backscatter," *ACM SIGCOMM Comput. Commun. Rev.*, vol. 45, no. 4, pp. 283–296, Sep. 2015.

[7] G. Yang, Q. Zhang, and Y.-C. Liang, "Cooperative ambient backscatter communications for green Internet-of-Things," *IEEE Internet Things J.*, vol. 5, no. 2, pp. 1116–1130, Apr. 2018.

[8] J. Qian, A. N. Parks, J. R. Smith, F. Gao, and S. Jin, "IoT communications with M-PSK modulated ambient backscatter: Algorithm, analysis, and implementation," *IEEE Internet Things J.*, vol. 6, no. 1, pp. 844–855, Feb. 2019.

[9] G. Yang, Y.-C. Liang, R. Zhang, and Y. Pei, "Modulation in the air: Backscatter communication over ambient OFDM carrier," *IEEE Trans. Commun.*, vol. 66, no. 3, pp. 1219–1233, Mar. 2018.

[10] M. A. ElMossallamy, M. Pan, R. Jäntti, K. G. Seddik, G. Y. Li, and Z. Han, "Noncoherent backscatter communications over ambient OFDM signals," *IEEE Trans. Commun.*, vol. 67, no. 5, pp. 3597–3611, May 2019.

[11] D. Darsena, "Noncoherent detection for ambient backscatter communications over OFDM signals," *IEEE Access*, vol. 7, pp. 159415–159425, Oct. 2019.

[12] A. Goldsmith, *Wireless Communications*. Cambridge, U.K.: Cambridge Univ. Press, 2005.

[13] A. F. Molisch, *Wireless Communications*, 2nd ed. Hoboken, NJ, USA: Wiley, 2011.

[14] C. Xu, L. Yang, and P. Zhang, "Practical backscatter communication systems for battery-free Internet of Things: A tutorial and survey of recent research," *IEEE Signal Process. Mag.*, vol. 35, no. 5, pp. 16–27, Sep. 2018.

[15] C. C. W. Ruppel, "Acoustic wave filter technology—A review," *IEEE Trans. Ultrason., Ferroelectr., Freq. Control*, vol. 64, no. 9, pp. 1390–1400, Sep. 2017.

[16] D. C. Malocha, "SAW/BAW acoustoelectronic technology for filters and communication systems," in *Proc. IEEE 11th Annu. Wireless Microw. Technol. Conf.*, Apr. 2010, pp. 1–7.

[17] C. C. W. Ruppel, L. Reindl, and R. Weigel, "SAW devices and their wireless communications applications," *IEEE Microw. Mag.*, vol. 3, no. 2, pp. 65–71, Jun. 2002.
[18] T. Bauer, C. Eggs, K. Wagner, and P. Hagn, "A bright outlook for acoustic filtering: A new generation of very low-profile SAW, TC SAW, and BAW devices for module integration," *IEEE Microw. Mag.*, vol. 16, no. 7, pp. 73–81, Aug. 2015.
[19] D. Tse and P. Viswanath, *Fundamentals of Wireless Communication*, 1st ed. Cambridge, U.K.: Cambridge Univ. Press, 2005.
[20] P. Zellini, "On some properties of circulant matrices," *Linear Algebra Appl.*, vol. 26, pp. 31–43, Aug. 1979.
[21] H. Mheidat, M. Uysal, and N. Al-Dhahir, "Equalization techniques for distributed space-time block codes with amplify-and-forward relaying," *IEEE Trans. Signal Process.*, vol. 55, no. 5, pp. 1839–1852, May 2007.
[22] I. S. Gradshteyn and I. M. Ryzhik, *Table of Integrals, Series and Products*, 7th ed. New York, NY, USA: Academic, 2007.

TAKANORI HARA (Graduate Student Member, IEEE) received the B.E. and M.E. degrees in engineering from The University of Electro-Communications, Tokyo, Japan, in 2017 and 2019, respectively, where he is currently pursuing the Ph.D. degree. His current research interests include communication theory, channel coding, grant-free access, and information theory.

RYUHEI TAKAHASHI received the B.E. and M.E. degrees in engineering from The University of Electro-Communications, Tokyo, Japan, in 2018 and 2020, respectively. His current research interests include energy harvesting and ultra-low power communications systems.

KOJI ISHIBASHI (Senior Member, IEEE) received the B.E. and M.E. degrees in engineering from The University of Electro-Communications, Tokyo, Japan, in 2002 and 2004, respectively, and the Ph.D. degree in engineering from Yokohama National University, Yokohama, Japan, in 2007. From 2007 to 2012, he was an Assistant Professor with the Department of Electrical and Electronic Engineering, Shizuoka University, Hamamatsu, Japan. From 2010 to 2012, he was a Visiting Scholar with the School of Engineering and Applied Sciences, Harvard University, Cambridge, MA, USA. Since April 2012, he has been with the Advanced Wireless and Communication Research Center (AWCC), The University of Electro-Communications, where he is currently a Professor. His current research interests include grant-free access, cell-free architecture, millimeter-wave communications, energy harvesting communications, wireless power transfer, channel codes, signal processing, and information theory.